

UNCERTAINTY ANALYSIS OF THE AERODYNAMIC PERFORMANCE OF EVTOL PROPELLERS VIA REYNOLDS STRESS TENSOR PERTURBATION

Giulio Gori¹ & Alex Zanotti¹

¹Department of Aerospace Science and Technology, Politecnico di Milano, Via La Masa 34, 20156, Milano, Italy.

Abstract

We employ a naive parametrization mapping the eigenvalues of the Reynolds Stress Tensor in the RANS computational model to two independent and uniformly distributed random variables. The parametrization ensures the positive-definiteness of the tensor and it is exploited to forward propagate the uncertainty inherent the structure of the RANS turbulence closure to specific quantities of interest. The uncertainty propagation is attained efficiently by relying on the Polynomial Chaos Expansions technique. In this regards, the proposed approach falls within the class of so-called Eigenspace Perturbation Methods for uncertainty quantification. In the aim of assessing the main peculiarities of the proposed methodology, we first apply it to a simple test case i.e., the classical NACA 0012 airfoil. Next, we apply the whole machinery to the investigation of a single propeller typically employed in eVTOL vehicles, considering the airplane mode flight conditions. We then interpret the performance analysis with regards to the propagated uncertainty.

Keywords: eVTOL, uncertainty quantification, Eigenspace Perturbation Method, RANS, turbulence uncertainty

1. Introduction

Characterizing the aerodynamics of multirotor systems with application to advanced electric Vertical Take-off and Landing (eVTOL) aircraft is a complex task requiring advanced numerical tools. The popular Reynolds-Averaged Navier–Stokes (RANS) model for Computational Fluid Dynamics (CFD) is typically the preferred choice to carry out numerical simulations since it provides a reasonable trade-off between computational cost and accuracy. Unfortunately, the RANS equations require a turbulence closure modeling the Reynolds Stress Tensor (RST), a byproduct of the time-averaging of the Navier–Stokes equations. Typically, turbulence closures rely on strong inherent model-form assumptions which limit the fidelity of CFD predictions in a wide variety of applications [1]. The direct quantification of such fidelity limitations is generally intractable and requires a the use of advanced Uncertainty Quantification (UQ) techniques [2].

In this work, we build on top of the so-called Eigenspace Perturbation Method (EPM) [3, 4] or Eigenspace Perturbation Framework (EPF) [5]. The EPM was originally devised to provide informed estimates of the variability range of selected Quantity of Interest (QoIs) due to the uncertainty inherent the structure of the equations employed to reconstruct the RST. In a similar fashion, it is also employed to assess structural uncertainty of the sub-grid scale models in Large Eddy Simulations [6]. In practice, a perturbation is applied to the RST eigenspace at each CFD iteration. This modifies the modeling of turbulent phenomena and, ultimately, the predicted flow. To efficiently explore the range of uncertainty associated to CFD predictions, the standard EPM implementation requires the execution of five different simulations, each subject to a specific perturbation cleverly selected to explore extremal states of turbulence componentiality and production [7]. Eventually, the EPM provides only a reasonable estimation of the uncertainty range, but by no means serves the establishing of rigorous and provable bounds.

Lately, we record a significant number of scientific works devoted to improving the method or to expanding its capabilities. An interesting aspect concerns improving our understanding of the implications associated to the methodology. In this regard, Mishra et al. [8] establish the limit of physical plausibility of the applied perturbations. Matha et al. [5] shed light on non trivial implications inherent the implementations of the EPM into computer codes. Indeed, typical implementations entail the use of a moderation factor to modulate the perturbation in the aim of improving the stability of the CFD simulation. Possibly, the use of a moderation factor may lead to a loss of physical consistency and, to overcome the issue, the Authors in [5] establish additional physics-based constraints that the EPM procedure must fulfill. On a different page, Researchers have been working to couple the EPM with optimization strategies to devise design frameworks constrained to credible CFD predictions [9, 10, 11, 12, 13].

In literature, there exist a few works investigating possible sampling strategies to generate random realizations of the RST, see [14, 15, 16, 17]. These focus on the parametrisation of the RST eigenvalues, on the parametrization of the orientation of the eigenvector, or both. Here, we employ a naive parametrization mapping the barycentric coordinates of the RST eigenvalues to two independent and uniformly distributed random variables, and use it to forward propagate the structural uncertainty to the targeted Qols based on the construction of Polynomial Chaos Expansions (PCE).

To investigate the methodology, we first refer the classical two-dimensional NACA 0012 airfoil for which we provide a basic analysis and a preliminary assessment of the performance of PCE surrogates. Next, we apply the whole machinery to the investigation of a single propellers typically employed for eVTOL architectures, considering the airplane mode flight conditions [18]. The aim is to re-interpret the performance analysis in view of the uncertainty propagation carried out with the extended EPM.

This paper is structured as follows. Section 2 briefly recalls the fundamentals of the EPM and presents the sampling strategy applied to obtain random realizations of the RST. Section 3 presents the results obtained for two reference test cases namely, subsonic flow of air over a NACA0012 airfoil at a variable angle of attack and the single propeller. Eventually, Sec. 4 summarizes the investigation.

2. Problem Statement

The EPM [3, 4] serves the estimation of the L2 type uncertainty [1]. In the following, and for the Reader's convenience, we first recall the EPM main features. After, we discuss the proposed parametrization.

By definition, the RST $\langle u_i u_j \rangle$, with $i, j = \{1, 2, 3\}$, is positive semi-definite and must abide by a set of realizability conditions [19, 20]

$$\langle u_i u_i \rangle \ge 0, \quad \langle u_i u_i \rangle + \langle u_j u_j \rangle \ge |2\langle u_i u_j \rangle|, \quad \det(\langle u_i u_j \rangle) \ge 0.$$
 (1)

Note that we use the angular brackets to express the time-averaged quantity. The well-known RST decomposition into an anisotropy and a deviatoric part

$$\langle u_i u_j \rangle = 2k \left(b_{ij} + \frac{\delta_{ij}}{3} \right),$$
 (2)

leads to a mathematically convenient form, with realizability conditions (1) applying to the anisotropy tensor b_{ij} . In the expression above, k is the turbulent kinetic energy and δ_{ij} the Kronecker delta. The anisotropy tensor b_{ij} can be expressed in its spectral form $b_{ij} = v_{ik} \Lambda_{kl} v_{jl}$ (v_{ik} and v_{jl} are the left and the right eigenvectors, Λ_{kl} is a diagonal matrix containing the eigenvalues λ_i).

According to the EPM, perturbations of finite amplitude are applied to the RST eigenspace during the CFD solution iterations. Perturbations must be admissible in view of the realizability conditions (1). In the most general approach, perturbations increase or decrease the amount of turbulent kinetic energy (k), varying eigenvalues of the anisotropy tensor (Λ_{kl}^*) , or rotate the anisotropy tensor eigenvectors (v_{ik}^*) . Perturbations allow to explore the whole RST realizability space and hence provide a mean to estimate the uncertainty associated to the structure of the turbulence closure. The interested Reader is referred to [3, 4] for a thorough overview of the EPM. The Reader is also referred to Refs. [4, 21, 15] discussing the challenges associated to modeling the spatial variability of perturbations.

In its standard implementation e.g., within the SU2 open-source suite [22], the EPM relies on the approach described in [7]. Namely, it is assumed a uniform spatial perturbation of Λ_{kl}^* and ν_{ik}^* , while the perturbation of the k value is neglected. According to Sys. (1), three limiting states of turbulence componentiality can be attained by perturbing the tensor eigenvalues λ_i . These are labeled 1C, 2C and 3C, and correspond to the 1, 2, and 3-component (isotropic) turbulence, and can be visualized as the vertices of a triangular domain in a barycentric coordinate system, see Fig. 1. It is worth noting that the eigenvalue perturbation results into a shape deformation of the ellipsoid associated to the RST [6]. A perturbation can also be applied to the orientation of the RST eigenvectors with the effect of modulating the production of turbulent kinetic energy \mathscr{P} , see [7].

The simultaneous perturbation of the eigenvalues (1C, 2C and 3C) and eigenvectors (\mathcal{P}^{max} and \mathcal{P}^{min}) leads to five possible extremal combinations. Hereinafter, we will adopt the following labels \mathcal{P}^{max}_{1C} (PA), \mathcal{P}^{max}_{2C} (PB), 3C (PC), \mathcal{P}^{min}_{1C} (PD), \mathcal{P}^{min}_{2C} (PE), and (BS) to indicate the baseline model. Recall that \mathbf{x}_{3C} corresponds to isotropic turbulence componentiality, thus \mathcal{P}_{3C} is invariant to the rotation of the eigenvectors. In the typical EPM setting, the turbulent uncertainty estimates of a selected performance p are obtained by executing the five EPM solutions. Therefore, the difference among the upper and the lower predictions of the targeted QoI (a generic performance p) reads

$$\Delta = \max(p^{\mathsf{PA}}, p^{\mathsf{PB}}, p^{\mathsf{PC}}, p^{\mathsf{PD}}, p^{\mathsf{PE}}) - \min(p^{\mathsf{PA}}, p^{\mathsf{PB}}, p^{\mathsf{PC}}, p^{\mathsf{PD}}, p^{\mathsf{PE}}), \tag{3}$$

and represents an estimation of the RANS model trustworthiness. In the following, we neglect PD and PE because of a twofold motivation. First, the rotation of the RST eigenvector basis augments the dimensionality of the uncertainty space, leading to a substantial increase of the computational cost of the UQ analysis. Second, perturbing the orientation of the RST basis is critical because of its combined effect with the under-relaxation factor required to stabilize CFD simulations, see [5]. The implications of this latter aspect would render the UQ analysis questionable.

In the proposed setting, we employ a naive parametrization inspired by [23] to map the barycentric coordinates of the RST eigenvalues to two uniform i.i.d. variables (ξ_1 , ξ_2)

$$\xi_1 = \mathscr{U}(0,1),\tag{4}$$

$$\xi_2 = \mathscr{U}(0,1),\tag{5}$$

$$x_p = \left(1 - \sqrt{\xi_1}\right) x_{1C} + \sqrt{\xi_1} \left(1 - \xi_2\right) x_{2C} + \xi_2 \sqrt{\xi_1} x_{3C},\tag{6}$$

$$y_p = \left(1 - \sqrt{\xi_1}\right) y_{1C} + \sqrt{\xi_1} \left(1 - \xi_2\right) y_{2C} + \xi_2 \sqrt{\xi_1} x_{3C},\tag{7}$$

being $x_{1C}=(0.0,0.0)$, $x_{2C}=(1.0,0.0)$, and $x_{3C}=\left(0.5,\sqrt{3}/2\right)$. The mapping can be exploited to forward propagate the structural uncertainty to any targeted Qols e.g., using a plain Monte Carlo approach to sample the realizability triangle, see Fig. 1a. The Monte Carlo approach is straightforward to implement and it allows to reconstruct the full probability distribution of the Qols under the assumption of that the user is not capable of characterizing the epistemic uncertainty inherent the construction of the RST closure. Nonetheless, achieving the convergence of the Monte Carlo estimates is computationally demanding, if not intractable, in case the application of interest entails a complex and computationally expensive CFD model i.e., the eVTOL propellers presented in this paper. Therefore, more advanced and efficient UQ methods must be employed.

In this work, we employ an UQ approach based on the construction of a Polynomial Chaos Expansion (PCE) of the full CFD model [24], see also [25] for a complete overview. Namely, we build a PCE surrogate of the mapping between the random inputs $\xi = \{\xi_1, \xi_2\}$ of the full computational model and the targeted QoIs $o = o(\xi_i)$. By considering a finite set of orthonormal polynomials $\Psi_k(\xi_i)$

$$o(\xi) \doteq \sum_{k=0}^{\infty} c_k \Psi_k(\xi), \tag{8}$$

the task reduces to computing the unknown coefficients c_k of the truncated expansion. The polynomial basis $\Psi(\xi_i)$ is chosen according to the Askey scheme [26], which in case of uniformly distributed inputs indicates the use of Legendre polynomials. We therefore sample the realizability triangle at

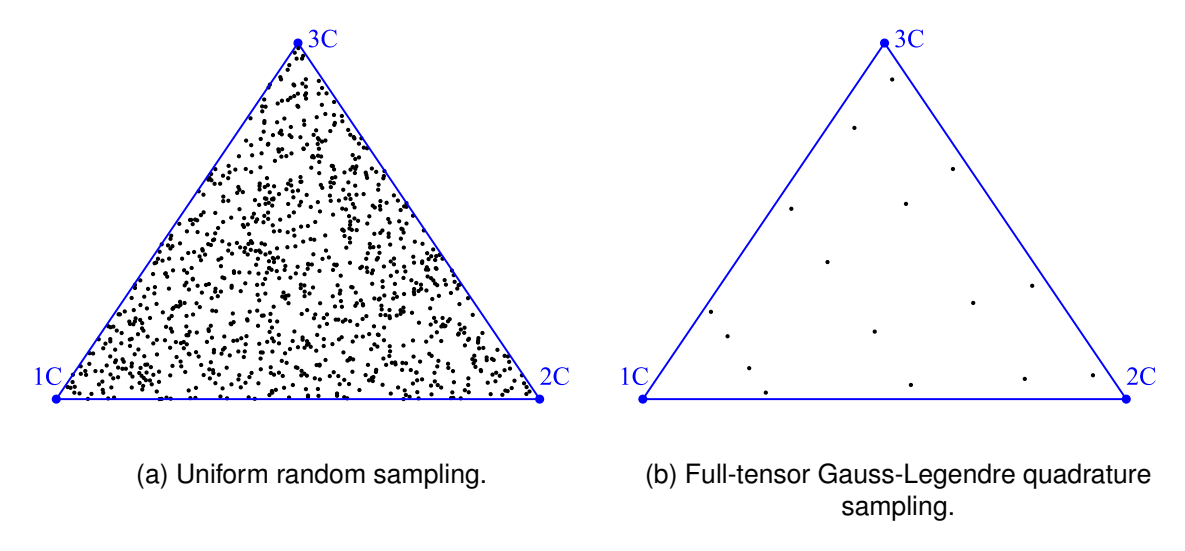


Figure 1 – Sampling over the eigenvalues realizability triangle (barycentric map)

the root of Legendre polynomials, see Fig. 1b, to solve a quadrature integration formula and compute the expansion coefficients. The PCE training set includes a total of 16 points (4 points on each uncertain dimension) and it allows to integrate exactly polynomials of order 3. The reason why we refer to the proposed mapping as naive lies in the fact that, although the random points are actually uniformly distributed over the triangle, points obtained from a regular spaced grid defined over ξ have unusual artifacts and do not look nicely distributed i.e., certain regions are more densely populated. Rigorously, one should employ a Dirichlet distribution defined over the 2-dimensional simplex, but this would entail three uncertain parameters whereas the naive method allows the parametrization based on two variables only. As shown later, the naive parametrization is nonetheless suited to the construction of high quality PCE surrogates.

As suggested in Ref. [27], the quality of the so-obtained PCE surrogates is assessed according to two error estimators. Namely, the first is the generalization error (Err_{gen}) defined as

$$\mathsf{Err}_{gen} = \left[\frac{1}{M} \sum_{i=1}^{M} \left(o(\xi_i) - \sum_{k=0}^{P} c_k \Psi_k(\xi_i) \right)^2 \right], \tag{9}$$

i.e., the expected value of the residual computed w.r.t. a validation test set of M=50 points randomly sampled from the realizability space. The second error estimator is the coefficient of determination (R²)

$$R^2 = 1 - \frac{\mathsf{Err}_{gen}}{\mathsf{Var}(\mathbf{O})},\tag{10}$$

being $\mathbf{O} = \{o_1, \dots, o_M\}$ the set of validation data and Var their empirical variance. In particular, $\mathsf{R}^2 \in (-\infty, 1]$ with the upper bound attained for perfect fit.

3. Results

3.1 Application to the simulation of a NACA0012 airfoil

This numerical experiment is employed to test the UQ analysis framework and corresponds to the 2DN00 validation case provided by the NASA TMR (Turbulence Modeling Resource) [28, 29].

The geometry consists in the popular NACA 0012 airfoil, see Fig. 2(a). The airfoil is operating in subsonic conditions at a Reynolds number (Re) of $6 \cdot 10^6$. The NASA TMR [28, 29] provides all the details concerning the geometry and the operating conditions. Solver specific settings include the assignment of a constant Prandtl number and the use of the Sutherland law to evaluate the local thermal conductivity and viscosity values, respectively. Concerning the boundary conditions, a turbulent to laminar viscosity ratio of 10.0 and a 5% intensity of turbulent fluctuation are applied at the farfield, whereas an adiabatic no-slip boundary condition apply on the airfoil surface.

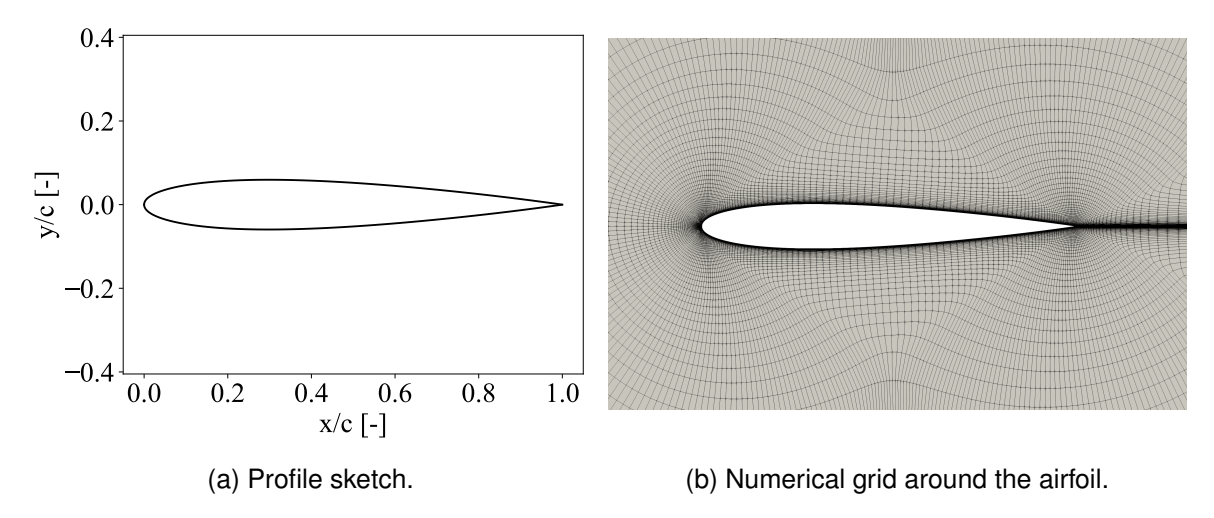


Figure 2 – NACA0012 baseline geometry.

CFD simulations are carried out using the open-source SU2 suite, see [30, 31]. The SU2 CFD solver is equipped with EPM capabilities [22] and, since its source code can be modified openly, it represents the best option for achieving the purposes pursued in this work. In SU2, the EPM is implemented considering the Menter's Shear Stress Transport (SST) closure [32] as the baseline closure (BS). Simulations are performed using a standard implicit time-marching approach. Second order accuracy is attained using a generalized Approximate Riemann solver of Roe type with a Monotone Upstream-centered Scheme for Conservation Laws (MUSCL) [33] in combination with the Venkatakrishnan limiter. First, the analysis targets the airfoil *lift coefficient* (c_l) and the *drag coefficient* (c_d).

The computational grid is provided by the [28, 29] (FAMILY I, 257 points on the airfoil surface). This choice is deemed a sufficient trade-off between maintaining an affordable computational cost and capturing the main flow features. The structure of the grid around the airfoil is shown in Fig. 2(b). Note that applying a perturbation to the RST is basically equivalent to changing the physics underlying the turbulence closure [34]. Therefore, a mesh sensitivity analysis should be performed independently for each EPM realization, to ensure that the CFD solution does not suffer from any dependency on the grid resolution. Because of this, the grid should be adapted to ensure the capturing of flow features peculiar to the specific EPM perturbation. Nonetheless, the computational burden would be unbearable and we accept the limitations.

The convergence of each simulation is monitored by evaluating integral quantities. Namely, we consider the c_l and c_d coefficients and adopt a Cauchy series approach. We consider the relative difference of the coefficients between relative iterations. When these are steady to a specified decimal place (10^{-6}) for a certain number (100) of consecutive iterations the simulation stops. If convergence criteria are not satisfied within 3000 CFD iterations, simulations are terminated forcefully (anyways, an a posteriori check confirmed that this maximum iterations limit is never achieved in the generation of the datasets exploited in the following).

We now present the UQ analysis. First, we show a qualitative example of the different flow configurations resulting from the BS model and from the application of the standard EPM perturbations (PA, PB, PC). Figures 3 show the Mach fields and the fields streamlines for the airfoil at $\alpha=20^\circ$. The BS closure produces a partially separated region in the aft part of the airfoil. The EPM models produce instead different solutions which include a fully attached flow (PA) and a largely separated region (PC). Naturally, using a diverse EPM model lead to a peculiar prediction of the stall onset. Note that experiments measure the onset of stall at about 17° - 18° . In general, one may provide a physical justification of these differences in view of the extremal states sought by the standard EPM. For instance, PA is designed to force all the turbulent kinetic energy in one single mode while the modeled Reynolds stress shares its eigendirections with the mean rate of strain tensor. The expected effect would be to delay stall. Nonetheless, we stress we are relying on a mesh selected to maintain the computational burden of the UQ analysis reasonable. Therefore, we refrain from providing any physical interpretation of the solution associated to a particular realization of the RST and focus on the

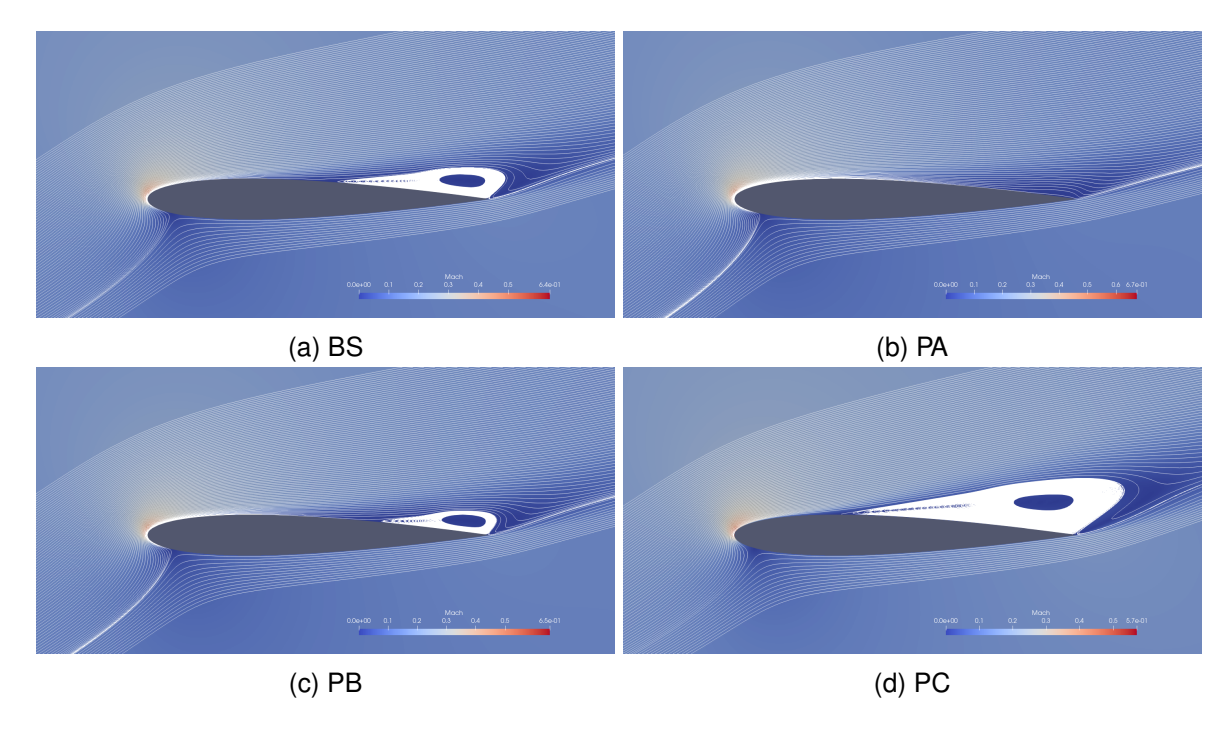


Figure 3 – NACA0012 Mach field and streamlines.

analysis of the uncertainty estimates.

Starting from here, we build PCE surrogates based on the full tensorization of the uncertainty space which entails 16 data points i.e., the 16 (ξ_1, ξ_2) tuples plot in Fig. 1b, and evaluate the statistics of the selected Qols. As we are in the process of evaluating the proposed UQ methodology, we also perform a Monte Carlo analysis (MC) entailing 1000 data points sampled randomly within the realization triangle, to produce benchmark data and assess the reliability of the PCEs. The surrogate quality assessment is reported in Fig. 4, showing the Err_{gen} and the R² indicators for both c_l and c_d at the different angles of attack. The indicators are computed w.r.t. both the PCE training and the MC data sets (this latter acting as a validation data set). Overall, surrogates are of good quality and prove their ability in mimicking the behavior of the full CFD model for any realization of the RST eigenvalues. Indeed, the generalizaiton error is always limited to very small values, whereas the coefficient of determination is practically always close to the best fit value.

The mean (μ) and the standard deviation (σ) of the targeted QoIs are computed from both the PCE and the MC analysis. Table 1 reports the quantitative analysis of the results obtained, to provide a quantitative comparison. In terms of statistics, the PCEs is confirmed to provide an excellent approximation of μ and σ for basically the whole α range (not all the α values are reported in the table).

For low α , a very small performance variability is observed. The mean performances from the UQ analysis is comparable to the nominal value of the BS closure, and this is fairly true also w.r.t. the PA, PB, and PC realizations. The 1- σ is quite limited and slightly lower than Δ (which is anyway significantly small considered the magnitude of the injected perturbations PA, PB, and PC). Not surprisingly, for low α the analysis indicates that the flow is basically insensitive to the employed RST closure. For higher values of α we obtain larger Δ and σ . Nonetheless, the former is about 5 times the latter, indicating that the standard EPM is very conservative.

To better appreciate the implications stemming from the use of the EPM, we report the comparison of the various closures and credibilty indicators in Fig. 5. The extremal EPM perturbations define a range including the BS, the μ_{MC} , and the μ_{MC} , which are in a fair agreement for both c_l and c_d . Even though the bulk of the MC realizations lies within the Δ envelope, we remind that the standard EPM does not provide rigorous and provable bounds.

The mean predictions from the MC and the PCE analysis almost overlap to the BS curve, if not for just very large values of α . We are not claiming here the general validity of that the BS prediction coincides with μ_{MC} (or μ_{PCE}). Indeed, for $\alpha=18-20^{\circ}$ a small discrepancy is noticeable in between the

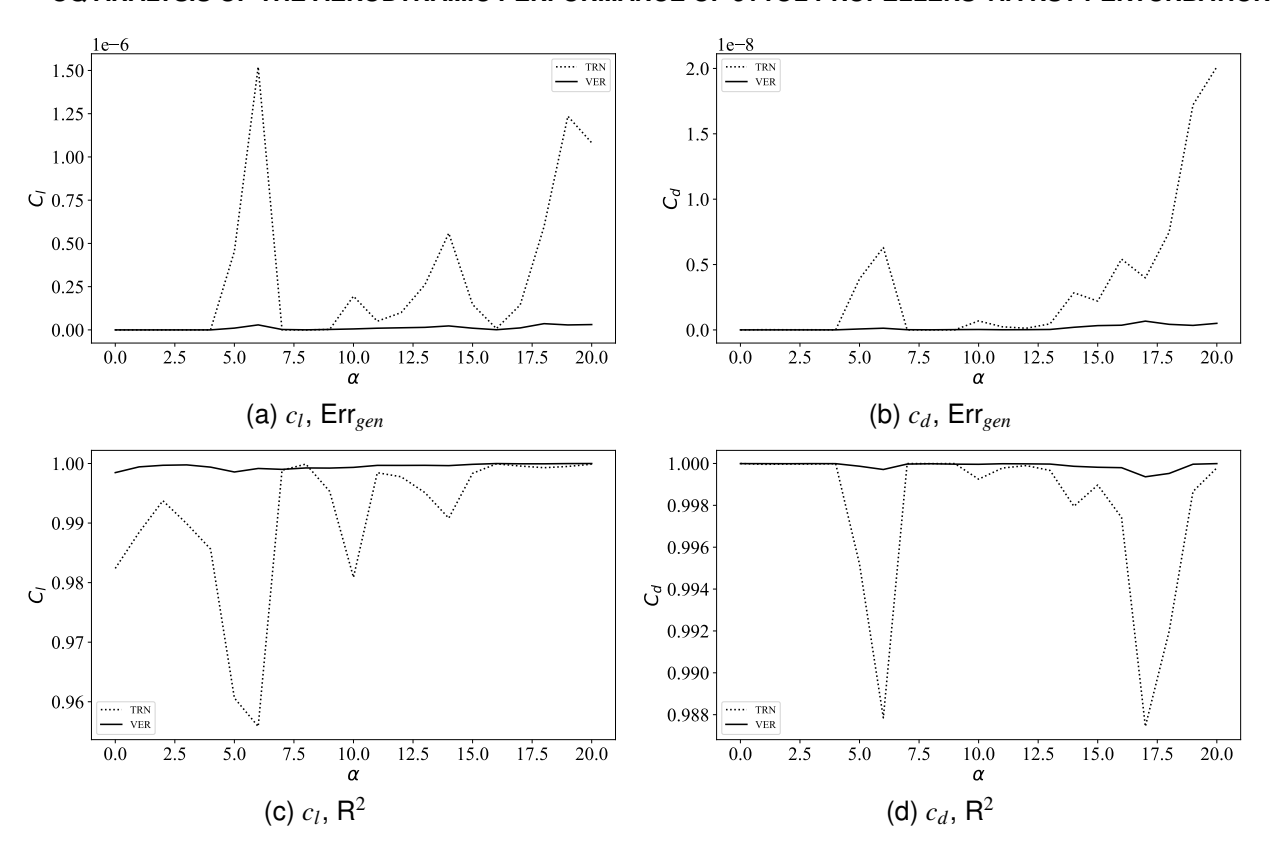


Figure 4 – NACA0012 PCE quality assessment.

curves. In particular, there is evidence of applications (not reported here) for which the μ prediction of a QoI does not corresponds to the BS solution e.g., the reattachment point of a separation bubble in a backward facing step. Anyways, the goal here is not to focus on the physics of the flow, but rather to assess the validity of the PCE-based UQ analysis compared to the plain MC analysis. Moreover, we also assess the possibly large difference in between the indications provided by the standard EPM, which seeks only extremal states of turbulence componentiality, and the parametrization we propose to obtain a more comprehensive characterization of the CFD output uncertainty. Additionally, and according to standard practice, perturbed CFD simulations are carried out using a fixed CFD numerical setup. Rigorously, each EPM realization would require a proper setup and grid to capture the peculiar physics produced by the specific RST perturbation. This approach is of course too demanding but would be necessary if one is interested in fundamental physics aspects. Instead, this is not an issue concerning establishing the credibility of the CFD model. Eventually, the credibility indicators account not only for the structural uncertainty inherent the turbulence closure, but also for additional uncertainty arising from its combined effect with numerics.

Table 1 – NACA0012 PCE quality assessment, summary table.

		$\alpha = 5^{\circ}$		$\alpha = 10^{\circ}$		$\alpha = 15^{\circ}$		$\alpha=20^{\circ}$	
		c_l	c_d	c_l	c_d	c_l	c_d	c_l	c_d
МС	μ_{MC}	0.5654	0.0097	1.0961	0.0146	1.5508	0.0278	1.7172	0.0732
	σ_{MC}	0.0027	0.0007	0.0029	0.0009	0.0084	0.0014	0.0827	0.0083
PCE	μ_{PCE}	0.5658	0.0098	1.0962	0.0146	1.5504	0.0277	1.7167	0.0732
	$\sigma_{\sf PCE}$	0.0023	0.0008	0.0025	0.0009	0.0079	0.0013	0.0814	0.0082
BS		0.5628	0.0089	1.0950	0.0138	1.5425	0.0264	1.6788	0.0759
PA		0.5658	0.0119	1.1054	0.0176	1.5637	0.0311	1.8436	0.0642
PB		0.5627	0.0095	1.0954	0.0145	1.5471	0.0271	1.7402	0.0700
PC		0.5623	0.0082	1.0927	0.0129	1.5278	0.0257	1.4186	0.1070
Δ		0.0035	0.0037	0.0127	0.0047	0.0358	0.0053	0.4249	0.0428

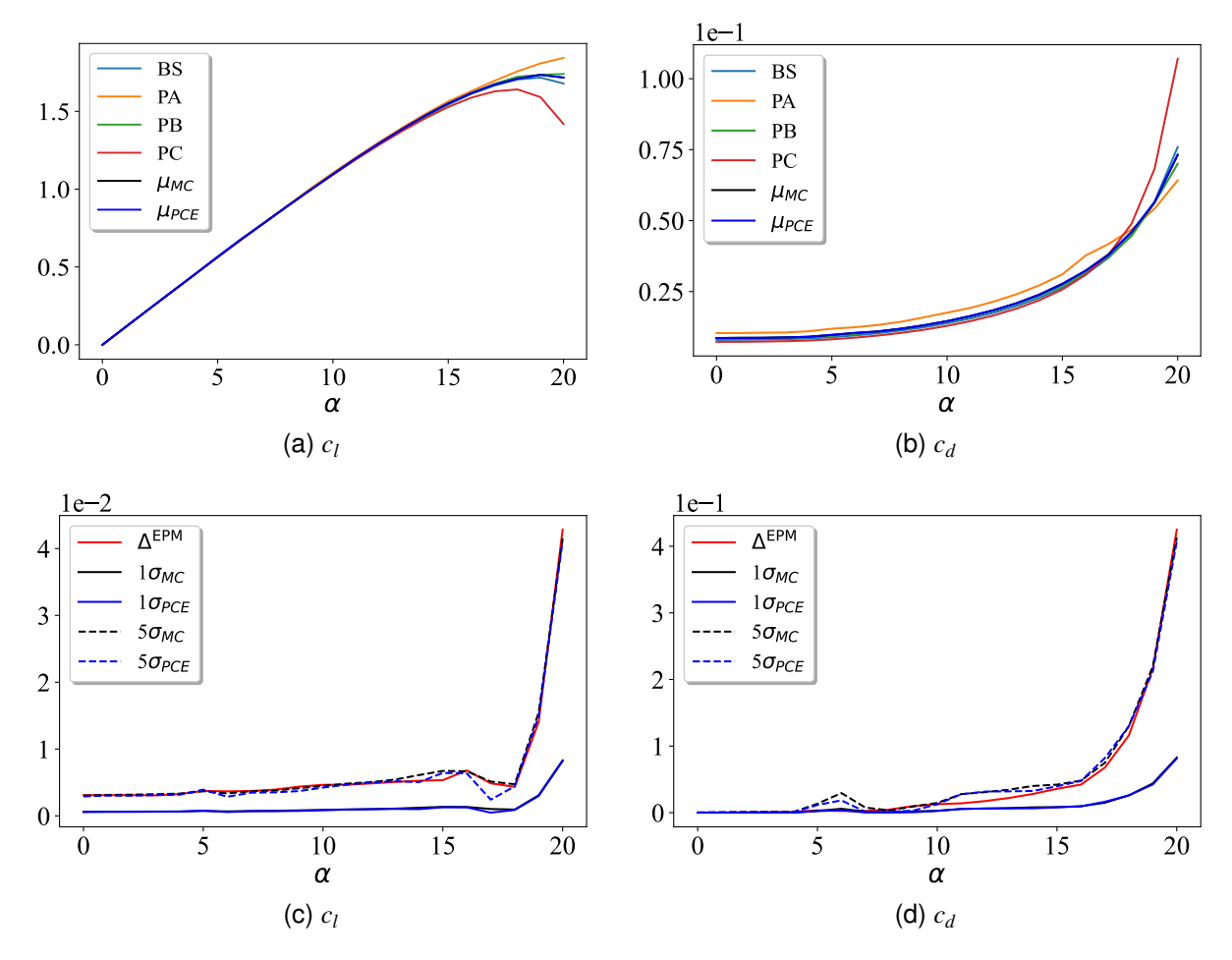


Figure 5 – NACA0012 UQ performance assessment.

In Figure 5 we also report a comparison of between the different credibility indicators. Both c_l and c_d plots reveal that, for the considered CFD model, Δ is significantly larger than σ_{PCE} i.e., same magnitude of the 5- σ_{PCE} range. For this CFD model, the conclusion is that the standard EPM implementation is quite conservative since it is unlikely, although in principle possible, for the true RST to fall outside the 5- σ_{PCE} range. We remind that we are not considering the perturbation of the eigenvectors, and that we are limiting the discussion to the eigenvalues only, therefore the discussion may be extended in the future.

Figure 6 reports the UQ analysis of the pressure and of the skin friction coefficients over the airfoil surface, as obtained for $\alpha = 5^{\circ}$, $\alpha = 10^{\circ}$, and $\alpha = 15^{\circ}$. For both QoIs, we report the BS prediction and the mean from the UQ analysis referred to the left ordinate axis. We refer the variability assessment to the right ordinate axis, reporting the standard Δ envelope and the 1- σ and 5- σ envelopes from the PCE analysis. The plots develop w.r.t. the curvilinear abscissa running anticlockwise from and to the trailing edge, being the x/c = 0.0 point the airfoil leading edge. Concerning the pressure coefficient, the μ prediction overlaps the BS one. This is true for all the considered values of α and, in general, for all the values in between the $0^{\circ} - 18^{\circ}$ range. Slight differences are found in the proximity of the leading edge for $\alpha = 19^{\circ}$ and $\alpha = 20^{\circ}$ (at such conditions, the airfoil is operating beyond the experimental stall angle and plots are not reported). We focus on investigating the variability of the c_n prediction. Practically, the prediction is less credible at the leading and trailing edges (in particular the former). For low values of the angle of attack, the extent of the EPM envelope is comparable to the $1-\sigma_{PCE}$. The EPM actually provides a limited range because the flow configuration is quite insensitive to the structural uncertainty in the turbulence closure. This is coherent with the fact that we are observing a QoI, the pressure coefficient of an airfoil at a low angle of attack, mostly determined by the configuration of the flow inviscid core. As α increases, turbulence begins to play a more relevant role and so does the uncertainty inherent the closure. Indeed, this is typically characterized by a

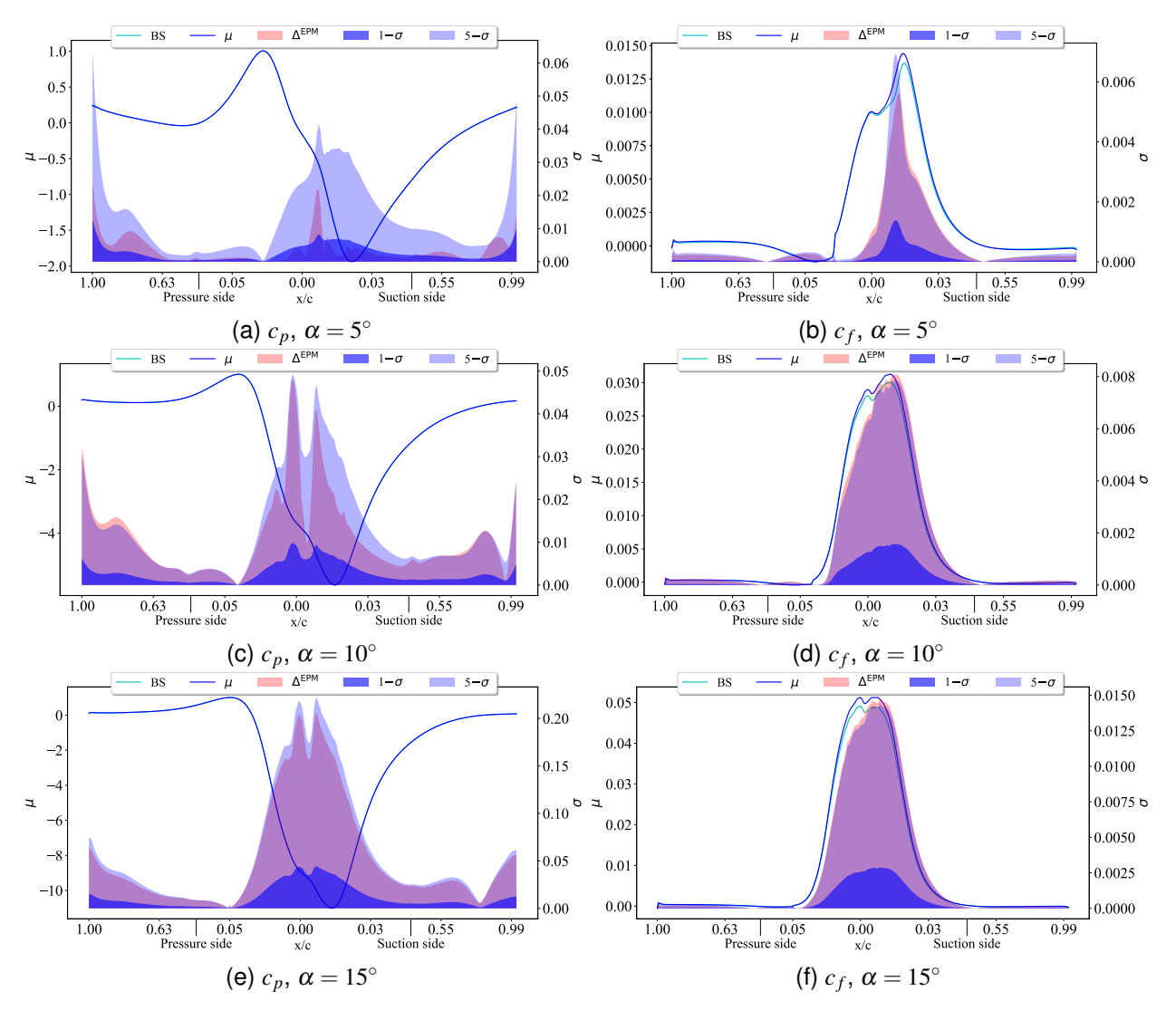


Figure 6 – NACA0012 UQ analysis of surface pressure and skin friction coefficients by means of PCE.

strong adverse pressure gradient and strongly curved streamlines, two conditions that are known to challenge the credibility of the RANS CFD model. The magnitude of the uncertainty envelopes increases, in particular the Δ which now covers the 5- σ_{PCE} interval.

The skin friction coefficient is instead subject to a different behavior. Indeed, the BS prediction differs from the UQ mean one in the proximity of the leading edge even for a low value of α . For $\alpha=5^{\circ}$, the extent of Δ is considerably large and again comparable with the 5- σ_{PCE} envelope. The sensitivity of the skin friction coefficient to the RST perturbation is reasonable since predictions strongly depend on the modeling of turbulence near the wall. For larger α , the BS- μ_{PCE} discrepancy at the leading edge is still present, with the magnitude of both σ_{PCE} and Δ increasing. In particular, the 1- σ_{PCE} uncertainty range is similar to the one resulting from the comparison of predictions from various turbulence closures reported in the NASA TMR.

For the observed test cases, including the results for the α values not reported here, Δ is significantly larger than the 1- σ_{PCE} envelope obtained from the proposed UQ framework. Namely, comparable to the 5- σ_{PCE} . Not surprisingly, the standard EPM turns out to be very conservative in establishing the credibility of the CFD model because it considers extremal states of turbulence componentiality which are hardly met in practical applications. Although the construction of PCE surrogates is more expensive than running just the extremal PA,PB, and PC, simulations i.e., it required the execution of 16 simulations in place of only 3, it provides a deeper insight concerning the uncertainty affecting the CFD model output. Moreover, once PCE of good quality are available, one may also exploit them to sample the uncertainty space and retrieve the full probability distribution characterizing the output.

3.2 Application to the simulation of a single propeller

We now present the UQ investigation concerning the aerodynamic performance of an isolated propeller. The propeller is designed for eVTOL applications: the geometry consists of the sole forward propeller from the tandem configuration designed and tested experimentally at Politecnico di Milano (PoliMI). The propeller is equipped with three left-handed VarioProp 12C blades for a disk diameter D=0.3 mm. A detailed description of the propeller and of the wind tunnel experiment for the full tandem configuration can be found in [35]. In brief, the summary of the conditions considered to carry out the UQ analysis is the following. The blades spin at 7050 RPM to produce a tip Mach number $M_t = 0.325$ which is typical for a full-scale eVTOL aircraft in cruise conditions with advance ratio $J = U_{\infty}/nD$ 0.8, being U_{∞} the free-stream velocity and n the rotor speed expressed in rev/s. The following freestream conditions apply: static pressure $p_{\infty} = 99600$ Pa, static temperature $T_{\infty} = 294.05$ K, and freestream density $\rho_{\infty} = 1.18 \text{ Kg/m}^3$. The freestream velocity is such that $M_{\infty} = 0.0820$, leading to a Reynolds number $Re = 1.96 \cdot 10^6$. The turbulence intensity is set at 0.1% upstream the propeller. The propeller is simulated using the RANS model from the open-source SU2 CFD suite and considering a steady rotating frame. The viscosity model assumes a uniform value of $1.716 \cdot 10^{-5}$ Pa·s throughout the whole domain. Numerical fluxes are discretized using the Jameson-Schmidt-Turkel (JST) scheme [36]. Gradients of the flow variables are reconstructed at the cell faces using the Green-Gauss method. Simulation convergence is monitored by assessing the evolution of the predicted torque coefficient during the iterates. Simulations are stopped once the coefficient is steady to the 10^{-6} decimal place for a 200 iterations. The numerical grid is built using the Pointwise software and covers only one-third of the volume around the propeller thanks to the exploitation of the geometry polar periodicity. Overall, the mesh includes about 2.3 million elements, with a maximum y^+ value of 1.8 at wall, and it is comparable to the *medium* mesh employed in [18]. A close-up view of the blade surface discretization of the Medium grid is shown in Fig. 7.

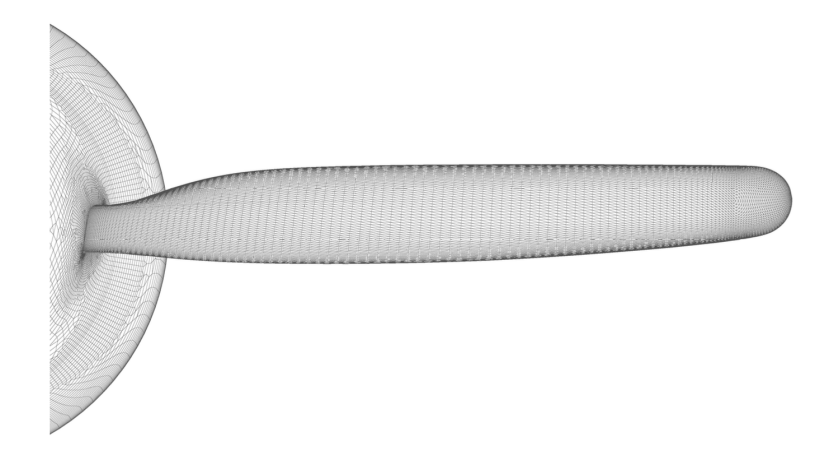


Figure 7 – S-PROPELLER. Close-up view of the blade surface mesh.

In the first place, the performances of the propeller are evaluated considering 3 different turbulence closures. Namely, we employ the one equation Spalart-Allmaras [37] closure with and without the algebraic BCM transition model [38], hereinafter labelled SAbcm and SA, respectively, and the two equations Menter's Shear Stress Transport closure [32], labelled BS. Table 2 reports the predicted performance coefficients obtained using the diverse turbulence closures and using the standard EPM approach. Note that the SST model is again the BS considered in the EPM. In particular, we compare the predicted thrust coefficient C_T and power coefficient C_P defined as:

$$c_T = \frac{T}{\rho_{\infty} n^2 D^4},\tag{11}$$

$$c_T = \frac{T}{\rho_{\infty} n^2 D^4},$$

$$c_P = \frac{P}{\rho_{\infty} n^3 D^5},$$
(11)

(13)

being T the thrust and P the power. From Tab. 2, it follows that the BS model leads to predictions

Table 2 – S-PROPELLER summary table.

		_	SAbcm	_	PA	PB	PC		μ_{PCE}	
			0.0948							
CP	0.107	0.1171	0.1025	0.1075	0.1164	0.1132	0.0870	0.0295	0.1112	0.0044

which fairly match the experimental measurement provided in [35]. The SA and the SAbcm either under/over estimate the observations. Nonetheless, the standard EPM provides a quite large uncertainty estimate Δ which practically includes all the turbulence closures' predictions.

Also for this test case, we build PCE surrogates of the QoIs according to the procedure described in Sec. 2. considering 16 training points and a validation data set of 50 randomly sampled points. Table 2 reports also the 1- σ_{PCE} value for comparison against Δ . The indication confirms the quite conservative information provided by the standard credibility estimator Δ .

In Figure 8, we report a graphical comparison of the dispersion of predictions provided by the different turbulence closures and EPM perturbations. In the same picture, we superimpose the experimental

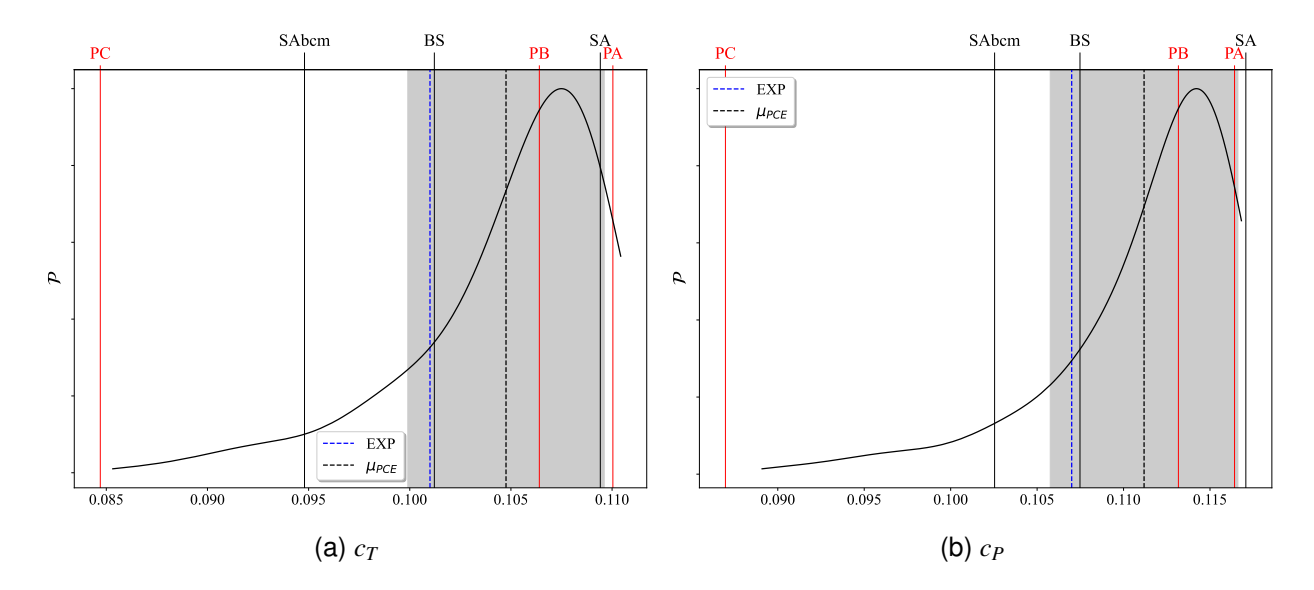


Figure 8 – S-PROPELLER UQ analysis of the thrust and power coefficients by means of PCE.

measurement (blue dashed line) and the mean (μ_{PCE} , black dashed line) and 1- σ_{PCE} envelope (gray shaded area) provided by the PCE-based UQ analysis. We also superimpose the full probability distribution reconstructed through a Monte Carlo analysis exploiting the PCE surrogates to predict the performance for random realizations of the RST. For both the c_T and c_P coefficients, the BS prediction is quite close to the experimental measure. The bulk of the probability distribution resulting from the UQ analysis is placed at values that slightly overestimate the experimental measure but, for both coefficients, the observation is included within the 1- σ_{PCE} envelope. Overall, probability distribution has a negative skew, with a long tail towards the lower values of the performance coefficients.

We remind that the UQ analysis is carried out sampling uniformly the whole realizability eigenvalues space, whereas the eigenvectors and the total amount of turbulent kinetic energy are still computed according to the BS model. In other words, because of the assumptions and of the implementation within the SU2 solver, the UQ results are not fully agnostic to the baseline turbulence closure. In this perspective, the μ_{PCE} value is representative of the mean prediction obtained assuming the minimum level of knowledge about the way energy is distributed among the different eigenmodes in the BS, being the 1- σ envelope an indicator of the dispersion of predictions around the mean value.

Not surprisingly, the standard EPM solutions are spread over a large range. In particular the upper boundary (PA) appears to be comparable to the $\mu_{PCE} + \sigma_{PCE}$ value. Instead, the lowest (PC) falls at the very far left end namely, on the tail of the probability distribution. Interestingly, the SA and SAbcm models provide predictions outside the 1- σ envelope indicating that the sole perturbation of the eigenvalues can unlikely explain the differences in the physics modeled by the different turbulence

closures.

Besides investigating the global aerodynamic performances of the propeller, we also analyse the uncertainty affecting the CFD model output w.r.t. the prediction of local surface quantities. The QoIs subject to UQ are the pressure distribution and the skin friction coefficient over the propeller surface. The quality assessment of the surrogates is reported in Fig. 9, where we report the forward and the lateral view of the propeller. Surrogates are of good quality. Namely, the generalization error is always

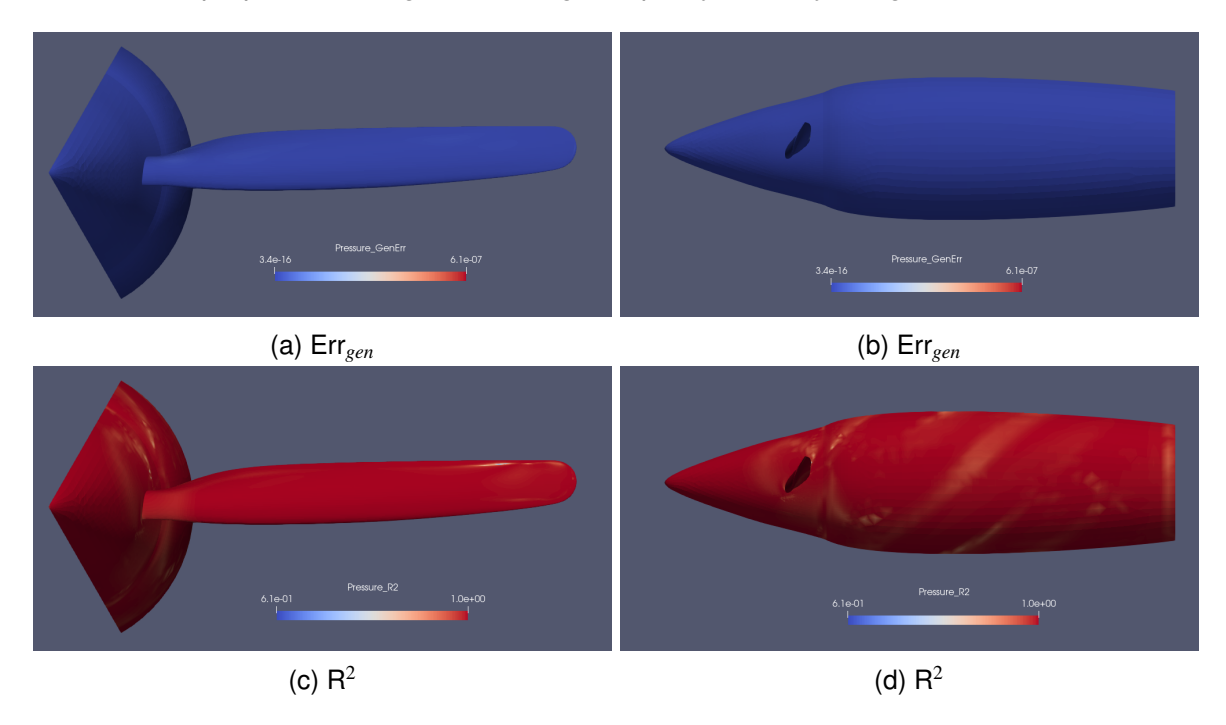


Figure 9 – S-PROPELLER. UQ analysis of static pressure by means of PCE.

below the $6.1\cdot 10^{-6}$ threshold, see Fig. 9a and Fig. 9b. The maximum relative error is recorded in a well defined region at the blade trailing edge, in the proximity of the hub junction. The coefficient of determination assumes instead a minimum value of 0.61 at the trailing edge of the blade tip, see Fig. 9c. Moreover, a certain loss of fit is recorded along the portion of the nacelle swept by the blade wake. Overall, the PCE surrogates are of good quality, suitable for the UQ analysis of the static pressure load over the propeller. We report the front and lateral view of the propeller coloured according to the average value of the normalized static pressure, in Fig. 10a and 10b. On average, the static pressure is lower at the blade tip and on the suction side, whereas it is larger on the pressure side, as expected. Figure 10c and 10d reports the 1- σ field over the propeller surface. The static pressure distribution on the nacelle is quite insensitive to the turbulence closure uncertainty. The frontal view shows that the pressure distribution over the blade is subject to a greater variability, with maximum uncertainty (about 6%) found at the trailing edge of the blade root section and on the outermost side of the tip. A medium variability is also present at different locations over the blade suction side, whereas the pressure side shows no significant variability.

We then present the UQ analysis of the skin friction coefficient over the propeller, in Fig. 11. The PCE quality assessment is not depicted for brevity reasons, but results confirm that the generalization error is always below the $1.7 \cdot 10^{-8}$ threshold, whereas the coefficient of determination ranges between 0.63 and 1.0, having a perfect fit in most of the surface. The mean skin friction reported in Figs. 11a and 11b highlights peak values at the leading edge of the blade, and particularly in the tip region. Note that the color scale does not cover the full extent of the mean value, but the range is selected to enhance the identification of the diverse zones which otherwise would be indistinguishable. On the rest of the surface, its magnitude diminishes to lower values. The variability related to the structural uncertainty in the turbulence closure is reported in Figs. 11c and 11d, which depict the 1- σ value over the surface. The largest uncertainty is associated to the prediction of the skin friction coefficient on the suction side, in proximity of the blade tip. The variability indicates that, in such regions, RANS predictions loose credibility and there the actual skin friction value may vary within a quite significant

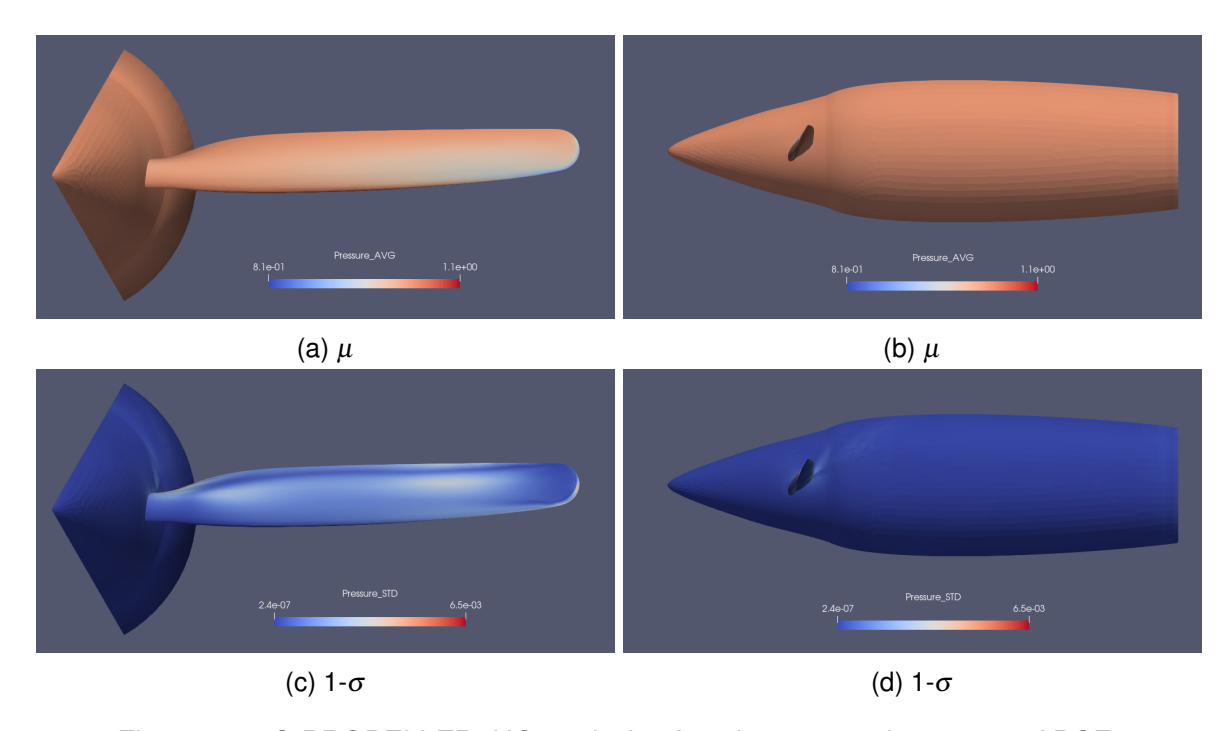


Figure 10 – S-PROPELLER. UQ analysis of static pressure by means of PCE.

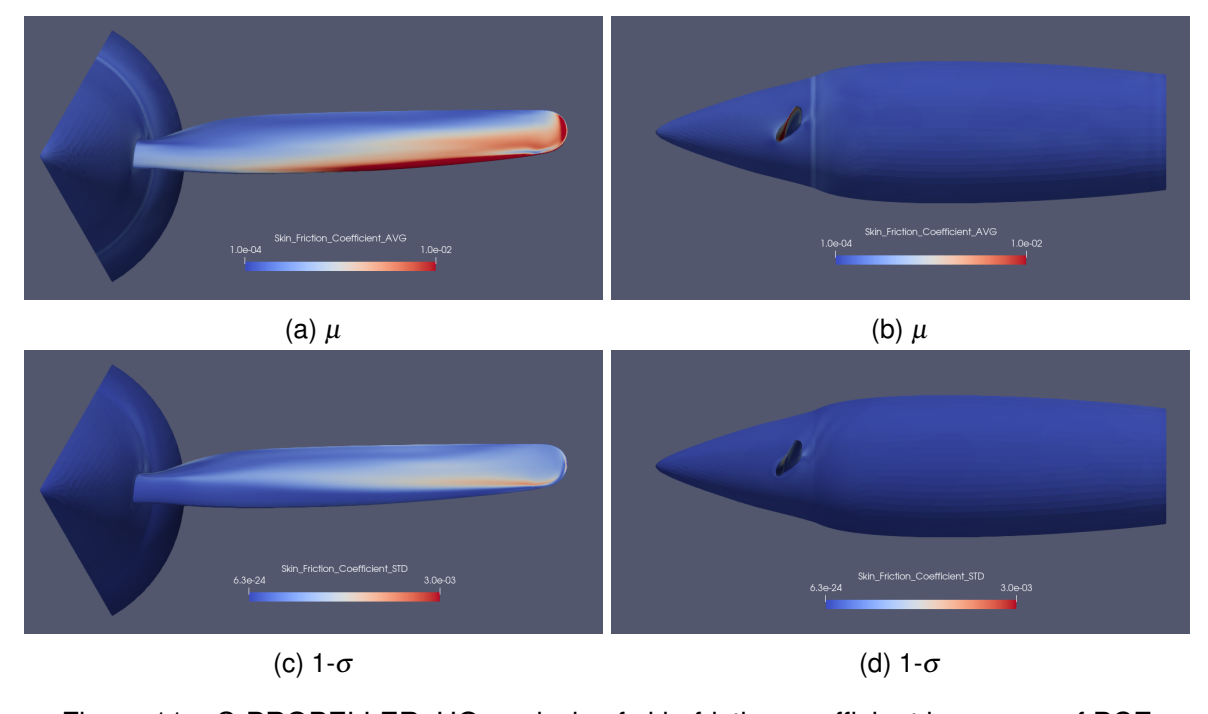


Figure 11 - S-PROPELLER. UQ analysis of skin friction coefficient by means of PCE

range.

On a similar path, we take advantage of numerical predictions to possibly estimate the uncertainty affecting the location of the separation line. Namely, we postprocess the solution to identify the region at which the surface trajectories defined by the skin friction vector field converge. To do so, we simplify the problem by considering blade chordwise sections. For each grid node, we project the skin friction vector on the plane normal to the blade span. In doing so, we enforce the strong assumption of that the spanwise component of the surface flow is negligible w.r.t. the prediction of the separation point. In practice, we retrieve the skin friction component tangent to the surface and normal to the blade span, and we investigate its orientation assigning a binary QoI (which can assume -1,1 value) depending on the direction i.e., from the leading to the trailing edge or viceversa. The PCE are trained to classify the RST realizations based on the expected direction of this so-defined QoI. We

stress that this procedure introduces a piece-wise approximation of the QoI over the blade surface. The consequence is that we introduce a jump discontinuity in the model that PCEs are trying to approximate. Nonetheless, the surrogates quality assessment reveals that the generalization error is below $7.8 \cdot 10^{-2}$, therefore negligible w.r.t. the -1,1 values, whereas $R^2 \ge 0.79$.

Figure 12 reports the $1-\sigma$ value associated to the prediction of the binary QoI due to the structural uncertainty in the RST approximation. The figures focus the analysis on the blade suction and pressure sides. Low variance indicates regions in which the chordwise component of the skin friction vector has the same direction irrespective of the perturbation applied to the RST. On the other hand, high variability indicates regions in which the orientation of the skin friction depend on the specific realization of the RST. Since the analysis of the nominal value assumed by the binary QoI reveals that the flow direction at the trailing edge is generally opposite to the one at the leading edge for the almost the whole blade span, it follows that regions of high variability are also critical concerning flow separation.

Figure 12 reports also the flow trajectory associated to the skin friction vector field on the blade surface. These are computed for three different nominal turbulence models i.e., the BS, SA, and SAbcm, and superimposed to the 1- σ field. Concerning the BS closure in Fig. 12a, we can appreciate that the trajectories converge in the proximity of the highest variability region for both the pressure and the suction sides. This is not surprising since the UQ analysis uses this closure as the baseline for the EPM, but also not trivial given the nonlinear character of the RANS equations.

Similarly, in Fig. 12b we report the surface trajectories stemming from the SA model. Also in this case the trajectories converge within the region of highest variability, for both the pressure and the suction sides, and this is not trivial given the substantial differences between SA and BS. Note that we are only investigating the direction of the surface friction vector, not its magnitude because the information is lost in the postprocessing.

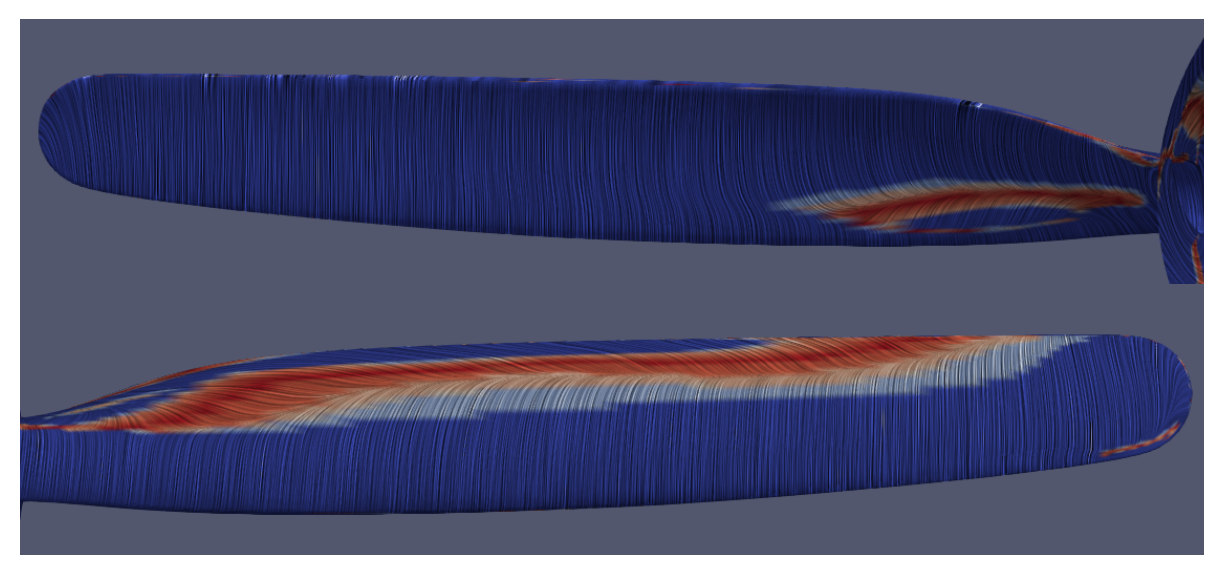
Lastly, Fig. 12c reports the trajectories provided by the SAbcm closure. The transition model implemented in this closure changes the physics of the flow significantly, particularly on the pressure side. Now trajectories converge in regions of low prediction variability, indicating a physics that can not be captured by the sole perturbation of the RST eigenvalues. Possibly, the perturbation of the eigenvectors should result in an enlargement of the uncertainty region and lead to including the SAbcm separation line.

4. Conclusions

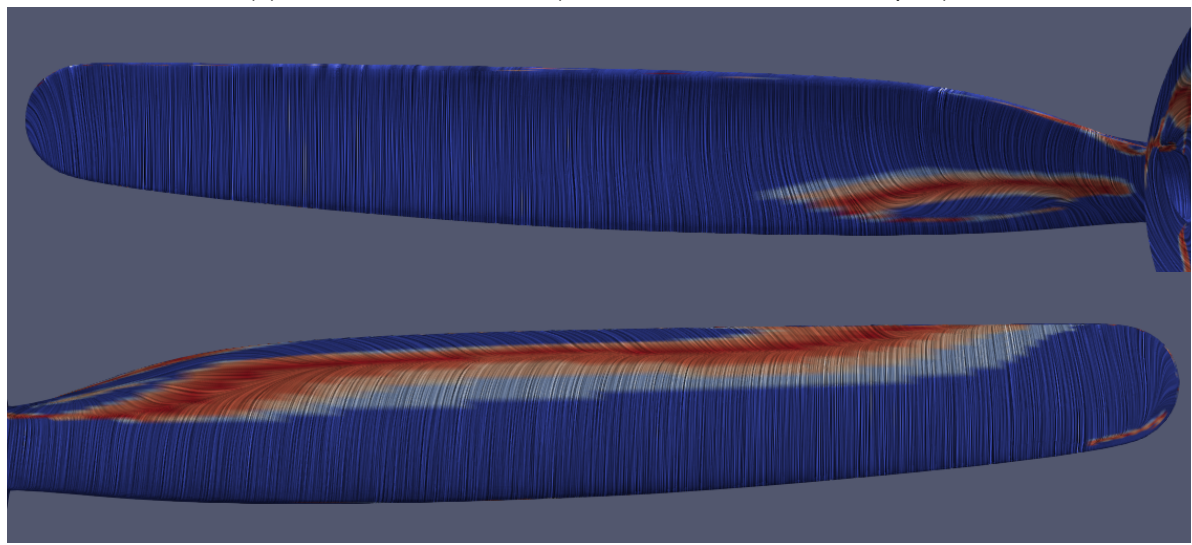
We employ a naive parametrization of the realizability space inherent the positive-definite definition of the RST tensor in the RANS CFD model.

The parametrization maps the RST eigenvalues to two random independent and uniformly distributed variables which are exploited to explore the realizability space and assess CFD prediction variability due to the structural uncertainty inherent the employed turbulence closure. A Polynomial Chaosbased approach is exploited to efficiently forward propagate the structural uncertainty to some targeted Qols. First, we present the UQ analysis of the performances of the well-known NACA0012 airfoil. This test case of low computational burden is provided mostly to present the UQ framework, to verify the feasibility and correctness of the approach w.r.t. a plain Monte Carlo analysis. For the observed test, standard EPM results to be very conservative, also in view of the fact that it explores extremal states of turbulence componentiality which are hardly met in reality. Overall, the comparison between the Monte Carlo and the PCE-based UQ analyses confirms the reliability of the framework proposed to characterize the output variability.

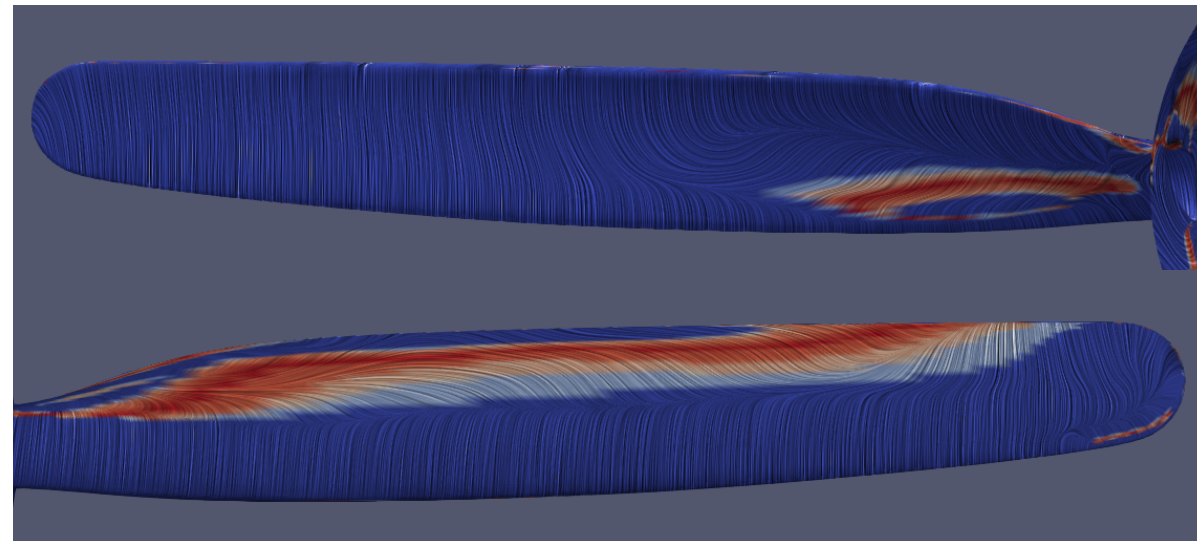
Secondly, we present the PCE-based UQ analysis of the performances of a single propeller typically employed in eVTOL applications. Despite the complexity of the application, it is shown that it is possible to build PCE surrogates of good quality, with limited generalization error and good fit score. The PCE-based analysis reveals that the structural uncertainty inherent to the energy partition between the three RST eigenmodes causes a limited variability of the global aerodynamic performances i.e., produced thrust and absorbed power. Concerning the CFD prediction of flow properties over the geometry surface, the UQ analysis highlights specific critical regions subject to uncertainty. In particular, for the static pressure these are the tip region and the mid portion of the blade suction side. Concerning the prediction of skin friction coefficient, the critical region is identified in the leading edge in



(a) BS turbulence closure (Menter's Shear Stress Transport)



(b) SA turbulence closure (Spalart-Allmaras)



(c) SAbcm turbulence closure (Spalart-Allmaras with algebraic BCM transition model)

Figure 12 – S-PROPELLER. UQ analysis of the flow separation point. The heat map is proportional to the local 1- σ of binary QoI indicating the direction of the local surface skin friction. Streamlines indicate the flow surface trajectory predicted using a specific turbulence closure.

the proximity of the blade tip. We also carried out a UQ analysis targeting the flow separation mechanism and identified the surface regions in which the prediction of the separation point is challenging because of a high sensitivity of the CFD model to the employed turbulence closure. These are the aft portion of the suction side (along the whole span) and the aft portion of the pressure side at the root. The conclusions drown here are based only on the perturbation of the RST eigenvalues. Rigorously, one should also perturb the orientation of the eigenvectors. Although in literature there exist parametrization of the rotational degrees of freedom, which one is best suited to provide a thorough exploration of the uncertainty space is still an open question. Naturally, including this additional uncertainty source would increase the cost of building the PCE surrogates. Therefore, before setting off in quest, one should decide whether it is actually necessary to carry out a comprehensive UQ analysis rather than just relying on the (extremal) information provided by the standard EPM. Indeed, the construction of PCE surrogates is generally more expensive than running the extremal simulations from the standard EPM. On the other hand, building PCEs of good quality could provide a deeper insight concerning the uncertainty affecting the CFD model output e.g., it would allow to retrieve the full probability distribution characterizing the output through a Monte Carlo sampling using the surrogate model. Note that alternative methods exist to generate random realizations of the RST, see [14, 15, 16, 17]. Here, we are just adding one framework to the deck.

Concerning the application, the next goal would be to investigate a more complex test case. The ready-at-hand test is the tandem configuration of the eVTOL propeller i.e., two propellers aligned axially and considering a variable distance. In such test, the wake of the leading propeller runs over the second, causing strong aerodynamic interaction among the two elements. In such case, we expect the CFD solution to be highly sensitive to the turbulence closure employed in the simulation.

5. Acknowledgements

This work was funded by the European Union (Project 101059320 - UN-BIASED). Views and opinions expressed are however those of the author(s) only and do not necessarily reflect those of the European Union or the European Research Executive Agency. Neither the European Union nor the European Research Executive Agency can be held responsible for them.

The Author would like to thank Francesco Caccia and Andrea Rausa from the Department of Aerospace Science and Technology, Politecnico di Milano, Via La Masa 34, 20156, Milano, Italy, for providing the computational mesh and for helping in the generation of images.

6. Contact Author Email Address

giulio.gori@polimi.it, Department of Aerospace Science and Technology, Politecnico di Milano, Via La Masa 34, 20156, Milano, Italy.

7. Copyright Statement

The authors confirm that they, and/or their company or organization, hold copyright on all of the original material included in this paper. The authors also confirm that they have obtained permission, from the copyright holder of any third party material included in this paper, to publish it as part of their paper. The authors confirm that they give permission, or have obtained permission from the copyright holder of this paper, for the publication and distribution of this paper as part of the ICAS proceedings or as individual off-prints from the proceedings.

References

- [1] Duraisamy K, Iaccarino G, and Xiao H. Turbulence modeling in the age of data. *Annual Review of Fluid Mechanics*, 51, January 2019.
- [2] Xiao H and Cinnella P. Quantification of model uncertainty in RANS simulations: a review. *Progress in Aerospace Sciences*, 108:1–31, July 2019.
- [3] Emory M, Rene P, and laccarino G. Modeling structural uncertainties in Reynolds-averaged computations of shock/boundary layer interactions. *AIAA 2011-479. 49th AIAA Aerospace Sciences Meeting including the New Horizons Forum and Aerospace Exposition*, January 2011.
- [4] Emory M, Larsson J, and laccarino G. Modeling of structural uncertainties in Reynolds-Averaged Navier-Stokes closures. *Physics of Fluids*, 25(11):110822, 2013.

- [5] Matha M and Morsbach C. Improved self-consistency of the Reynolds stress tensor eigenspace perturbation for uncertainty quantification. *Physics of Fluids*, 35(6):065130, June 2023.
- [6] Jofre L, Domino S, and laccarino G. A framework for characterizing structural uncertainty in Large-Eddy Simulation closures. *Flow Turbulence Combust*, pages 341–363, August 2018.
- [7] Iaccarino G, Mishra A, and Ghili S. Eigenspace perturbations for uncertainty estimation of single-point turbulence closures. *Physical Review Fluids*, 2, February 2017.
- [8] Mishra AA and laccarino G. Theoretical analysis of tensor perturbations for uncertainty quantification of Reynolds averaged and subgrid scale closures. *Physics of Fluids*, 31(7):075101, July 2019.
- [9] Nassim R, Gori G, laccarino G, and Congedo PM. Optimization of an ORC supersonic nozzle under epistemic uncertainties due to turbulence models. *GPPS 2019 Global Power and Propulsion Society*, Januar 2019.
- [10] Cook L, Mishra A, Jarrett J, Willcox K, and Iaccarino G. Optimization under turbulence model uncertainty for aerospace design. *Physics of Fluids*, 31:105111, October 2019.
- [11] Mishra AA, Mukhopadhaya J, Alonso JJ, and laccarino G. Design exploration and optimization under uncertainty. *Physics of Fluids*, 32(8):085106, August 2020.
- [12] Li A, Wang T, Chen J, Huang Z, and Xi G. Adjoint design optimization under the uncertainty quantification of Reynolds-Averaged Navier-Stokes turbulence model. *AIAA Journal*, pages 1–12, 2024.
- [13] Gori G, Le Maître OP, and Congedo PM. A confidence-based aerospace design approach robust to structural turbulence closure uncertainty. *Computers & Fluids*, 246:105614, 2022.
- [14] Huang Z, Mishra A, and Iaccarino G. A nonuniform perturbation to quantify RANS model uncertainties. *Center for Turbulence Research Annual Research Briefs, Stanford Univ., Stanford, CA*, pages 223–232, 2020.
- [15] Xiao H, Wu JL, Wang JX, Sun R, and Roy CJ. Quantifying and reducing model-form uncertainties in Reynolds-Averaged Navier–Stokes simulations: A data-driven, physics-informed Bayesian approach. *Journal of Computational Physics*, 324:115–136, November 2016.
- [16] Xiao H, Wang JX, and Ghanem RG. A random matrix approach for quantifying model-form uncertainties in turbulence modeling. Computer Methods in Applied Mechanics and Engineering, 313:941–965, January 2017.
- [17] Wang JX, Sun R, and Xiao H. Quantification of uncertainties in turbulence modeling: A comparison of physics-based and random matrix theoretic approaches. *International Journal of Heat and Fluid Flow*, 62:577–592, December 2016.
- [18] Caccia F, Abergo L, Savino A, Myles M, Zhou BY, Gori G, Zanotti A, Gibertini G, Vigevano L, and Guardone A. Multi-fidelity numerical approach to aeroacoustics of tandem propellers in eVTOL airplane mode. *AIAA 2023-3221. AIAA Aviation 2023 Forum*, June 2023.
- [19] Simonsen AJ and Krogstad PA. Turbulent stress invariant analysis: Clarification of existing terminology. *Physics of Fluids*, 17(8):088103, August 2005.
- [20] Schumann U. Realizability of Reynolds-stress turbulence models. *Physics of Fluids*, 20(5):721–725, May 1977.
- [21] Gorlé C and laccarino G. A framework for epistemic uncertainty quantification of turbulent scalar flux models for Reynolds-averaged Navier-Stokes simulations. *Physics of Fluids*, 25(5):055105, 2013.
- [22] Mishra AA, Mukhopadhaya J, Iaccarino G, and Alonso JJ. An uncertainty estimation module for turbulence model predictions in SU2. *AIAA Journal*, 57(3):1066–1077, March 2019.
- [23] Osada R, Funkhouser T, Chazelle B, and Dobkin D. Shape distributions. *ACM Transactions on Graphics*, 21(4):807–832, October 2002.
- [24] Wiener N. The homogeneous chaos. American Journal of Mathematics, 60(4):897–936, October 1938.
- [25] Ghanem RG and Spanos PD. *Stochastic finite elements: a spectral approach*. Springer-Verlag, Berlin, Heidelberg, 1991.
- [26] Xiu D. Numerical methods for stochastic computations: A spectral method approach. *Princeton University Press*, 2010.
- [27] Sudret B. Polynomial chaos expansions and stochastic finite element methods. *Risk and Reliability in Geotechnical Engineering*, 2015.
- [28] NASA Langley Turbulence Modeling Resource website. http://turbmodels.larc.nasa.gov. Accessed: 2019-11-11.
- [29] Jespersen DC, Pulliam TH, and Childs ML. OVERFLOW: Turbulence modeling resource validation results. NASA Technical Report, (NASA-2016-01), 2010.
- [30] Palacios F, Alonso JJ, Duraisamy K, Colonno M, Hicken J, Aranake A, Campos A, Copeland S, Economon

- TD, Lonkar A, Lukaczyk T, and Taylor T. Stanford University Unstructured (SU²): An open-source integrated computational environment for multi-physics simulation and design. *AIAA 2013-287. 51st AIAA Aerospace Sciences Meeting including the New Horizons Forum and Aerospace Exposition*, January 2013.
- [31] Economon TD, Mudigere D, Bansal G, Heinecke A, Palacios F, Park J, Smelyanskiy M, Alonso JJ, and Dubey P. Performance optimizations for scalable implicit RANS calculations with SU2. *Computers & Fluids*, 129:146–158, 2016.
- [32] Menter F. Zonal two equation k-w turbulence models for aerodynamic flows. *AIAA 1993-2906. 23rd Fluid Dynamics, Plasmadynamics, and Lasers Conference*, July 1993.
- [33] van Leer B. Towards the ultimate conservative difference scheme. V. A second-order sequel to Godunov's method. *Journal of Computational Physics*, 32(1):101–136, July 1979.
- [34] Gori G, Le Maître OP, and Congedo PM. On the sensitivity of structural turbulence uncertainty estimates to time and space resolution. *Computers & Fluids*, 229:105081, 2021.
- [35] Zanotti A and Algarotti D. Aerodynamic interaction between tandem overlapping propellers in eVTOL airplane mode flight condition. *Aerospace Science and Technology*, 124:107518, May 2022.
- [36] Jameson A, Schmidt W, and Turkel E. Numerical solution of the Euler equations by finite volume methods using Runge Kutta time stepping schemes. *AIAA 1981-1259. 14th Fluid and Plasma Dynamics Conference*, June 1981.
- [37] Spalart P and Allmaras S. A one-equation turbulence model for aerodynamic flows. *AIAA 1992-439. 30th Aerospace Sciences Meeting and Exhibit*, January 1992.
- [38] Cakmakcioglu SC, Bas O, Mura R, and Kaynak U. A revised one-equation transitional model for external aerodynamics. *AIAA 2020-2706, AIAA Aviation 2020 Forum*, June 2020.